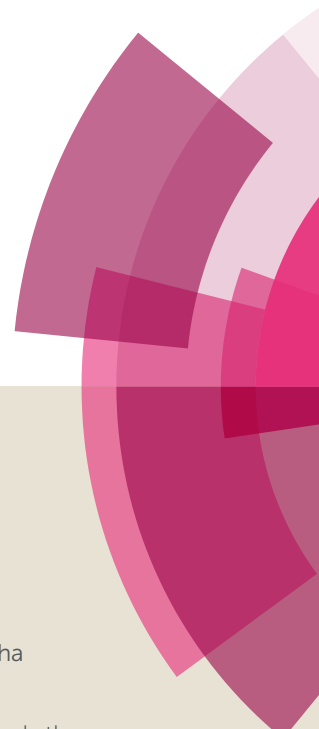


NJC

Accepted Manuscript



This article can be cited before page numbers have been issued, to do this please use: P. Ghosh, P. Saha and D. Samanta, *New J. Chem.*, 2016, DOI: 10.1039/C6NJ02903E.



This is an Accepted Manuscript, which has been through the Royal Society of Chemistry peer review process and has been accepted for publication.

Accepted Manuscripts are published online shortly after acceptance, before technical editing, formatting and proof reading. Using this free service, authors can make their results available to the community, in citable form, before we publish the edited article. We will replace this Accepted Manuscript with the edited and formatted Advance Article as soon as it is available.

You can find more information about Accepted Manuscripts in the [author guidelines](#).

Please note that technical editing may introduce minor changes to the text and/or graphics, which may alter content. The journal's standard [Terms & Conditions](#) and the ethical guidelines, outlined in our [author and reviewer resource centre](#), still apply. In no event shall the Royal Society of Chemistry be held responsible for any errors or omissions in this Accepted Manuscript or any consequences arising from the use of any information it contains.



Journal Name

ARTICLE

Glyoxalbis(2-methylmercaptoanil) complexes of nickel and ruthenium: radical versus non-radical states[†]

Pinaki Saha,^a Debasish Samanta^a and Prasanta Ghosh*^aReceived 00th January 20xx,
Accepted 00th January 20xx

DOI: 10.1039/x0xx00000x

www.rsc.org/

The coordination chemistry of a N₂S₂ donor α-diimine ligand, glyoxalbis(2-methylmercaptoanil) (gmma), with transition metal ions was explored. The study authenticated that gmma is a redox non-innocent flexidentate ligand. The nickel(II) and ruthenium(II) complexes of the types *trans*-[Ni^{II}(gmma)Cl₂] (**1**), *trans*-[Ru^{II}(gmma)Cl₂] (**2**) and [Ru^{II}(gmma)(PPh₃)Cl]Cl (**3**⁺Cl⁻) were isolated. Single crystal X-ray crystallography established that the diimine fragment particularly in **2** and **3**⁺Cl⁻·H₂O are severely distorted. EPR spectroscopy and density functional theory (DFT) calculations authenticated that the octahedral **1**⁻ and **1**²⁻ ions are gmma anion radical (gmma^{-•}) and gmma diimide (gmma²⁻) complexes of the types *trans*-[Ni^{II}(gmma^{-•})Cl₂]⁻ (**1**⁻) and *trans*-[Ni^{II}(gmma²⁻)Cl₂]²⁻ (**1**²⁻) which are unstable in solution. The chemically and electrochemically reduced ions undergo a chemical change to a dinuclear square planar nickel(II) complex of the type [(μ-NSNS-gmma)Ni₂Cl₃(PF₆)] (**4**^{PF₆}) in presence of PF₆⁻ salt, predicted by ESI mass spectroscopy, where μ-NSNS-gmma is a bis(methylthio-imine) donor bridging ligand. The CSS solution of **2** is stable. In contrast to **1**⁻ and **1**²⁻ ions, **2**⁻ in solution does not undergo any chemical change and it is defined as a resonance hybrid of *trans*-[Ru^{II}(gmma^{-•})Cl₂]⁻ and *trans*-[Ru^{III}(gmma²⁻)Cl₂]⁻ states. Similarly, **3** is defined as a resonance hybrid of [Ru^{II}(gmma^{-•})(PPh₃)Cl] and [Ru^{III}(gmma²⁻)(PPh₃)Cl] states. In **2**⁻ and **3** the atomic spin is delocalised over both ruthenium and the α-diimine fragment, authenticated by the unrestricted DFT calculations. The UV-vis absorption spectra of the isolated complexes and their reduced analogues were analyzed by spectroelectrochemical measurements and TD DFT calculations.

Introduction

The participation of the redox non-innocent ligands, either in paramagnetic or open shell singlet state, in different catalytic cycles has been documented.¹ The role of the redox non-innocent ligands in different forms to control catalytic reactions is disclosed.^{1d} It is noteworthy that a redox non-innocent ligand is an agent that can expand the activity of the central metal ion, particularly in cases of oxidative addition reactions.² The diverse activity of the redox non-innocent ligands thus is a tool to model functional coordination complexes. Sharing of an unpaired electron of a coordination complex by the metal ion as well as the ligand is not common

in coordination chemistry. A redox non-innocent chelate is an entity that can receive electron from the metal ion, can transfer electron to the metal ion and can share an electron with the metal ion. The first two phenomena induce the formation of organic radicals, whereas the third process will generate a state, in which the contributions of both radical and non-radical states are present. This particular state can be defined as a “resonance hybrid” (mixed character) of radical and non-radical states. Features of the organic radicals coordinated to transition metal ions as well as the resonance hybrid states are a subject of investigation.

Notably, the nickel complexes of aliphatic α-diimine which are redox non-innocent, emerge as promising catalysts for olefin polymerization and coupling reactions.³ Heterocyclic α-diimine complexes of ruthenium are numerous. The photo functionality and catalytic activities of these complexes were investigated in various aspects.⁴ However, the aliphatic α-diimine complexes of ruthenium are limited in scope and in this study α-diimine complexes of nickel and ruthenium were explored, particularly to define versatile electronic states containing ruthenium(II/III) ions and the neutral/mono and di-reduced diimine fragment. The α-diimine ligand of the type L^RR₂' that exists as neutral diimine (L^RR₂'), diimine anion radical (L^RR₂'^{-•}) and di-anionic diimide (L^RR₂'²⁻), as illustrated in Scheme 1 was persuaded in many cases to explore the anion

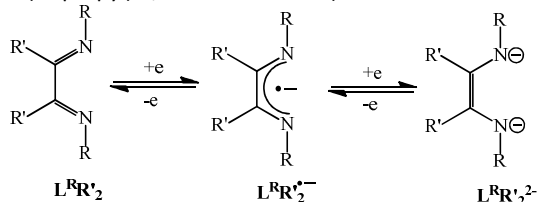
^a Department of Chemistry, R. K. Mission Residential College, Narendrapur, Kolkata-103, India. Email: ghosh@pghosh.in; Fax: +91 33 24773597

[†]Electronic Supplementary Information (ESI) available: X-ray crystallographic CIF files for the gmma, **1**·CH₂Cl₂, **2** and **3**⁺Cl⁻·H₂O; Electron transfer series of gma; Crystallographic data, Redox potential data; Mass spectrum of **4**^{PF₆}; Molecular geometry of gmma in crystal; EPR measurement parameters; Variable temperature EPR spectra of **2**⁻, **2**[•] and **3**; Optimized geometries of **1**²⁻ as (a) bis(methylthio-imine) donor and (b) NN-donor; Atomic spin of gmma^{-•}; Frontier molecular orbitals of **2**; Calculated excitation energies, oscillation strengths and transition types of gmma, **1**, **2**, and **3**^{Me⁺} obtained from TD DFT calculations in CH₂Cl₂; Spectroelectrochemical measurements of (a) **2** → **2**⁻ and (b) **2** → **2**[•] conversions in CH₂Cl₂ at 298 K; Gas phase optimized coordinates of gmma, gmma^{-•}, [Zn(gmma)Cl₂], **1**, **1**⁻, **1**²⁻, **2**, **2**[•], **2**[•], **3**^{Me⁺}, **3**^{Me⁺} and **3**^{Me⁺}. For ESI and crystallographic data in CIF files for the complexes see DOI: 10.1039/x0xx00000x

ARTICLE

Journal Name

radical states coordinated to transition metal ions.⁵ The bond parameters and the spectral features of these three electronic states, $L^R R_2'$, $L^R R_2'^{\bullet-}$ and $L^R R_2'^{2-}$ in complexes are significantly different. In this regard, electronic states of the members of the electron transfer series, $[Ni(L)]^z$ ($z = 0, 1+, 2+$; $L = 2$ -phenyl-1,4-bis(isopropyl)-1,4-diazabutadiene) are remarkable.^{6b-e}



Scheme 1 Redox series of α -diimine fragments.

Glyoxalbis(2-mercaptoanil) (gma) is a tetradentate ligand incorporating a stable diimine fragment which coordinates metal ion as a N_2S_2 -donor as shown in Scheme S1. The coordination chemistry of gma is rich and the elucidation of the electronic structures of the transition metal complexes of gma particularly with iron was a subject of research in last two decades.⁷ Eventually $gma^{\bullet-}$ anion radical complexes of iron(III/II) were successfully isolated.⁸ The investigation inferred that the gma is redox non-innocent. Similarly, the coordination chemistry of the redox non-innocent dianionic glyoxalbis(2-hydroxyanil) (gha) developed significantly.⁹

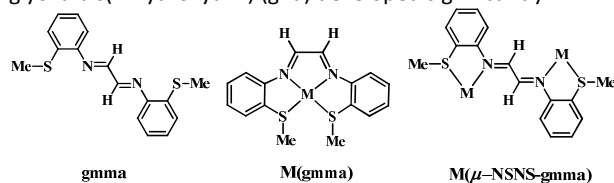


Chart 1 gmma ligand and the binding modes.

In this project, the coordination chemistry of glyoxalbis(2-methylmercaptoanil) (gmma) of nickel and ruthenium was investigated, to foster the uncommon nickel(I)-(α -diimine)/nickel(II)-(α -diimine anion radical) and ruthenium(II)-(α -diimine)/ruthenium(II)-(α -diimine anion radical)/ruthenium(III)-(α -diimide) states. The search disclosed that gmma is a redox non-innocent flexidentate ligand acting as a N_2S_2 -donor tetradentate ligand as gmma and bis(methylthioimine) donor bridging ligand as μ -NSNS-gmma as depicted in Chart 1. It is to be noted that a binuclear ruthenium(II) complex of μ -NSNS-gmma of the type $[(acac)_2Ru^II(\mu-NSNS-gmma)Ru^II(acac)_2]$ incorporating acetylacetonate (acac) as coligands was reported in a different aspect.¹⁰

Nickel(II) and ruthenium(II) complexes of gmma of the types $trans-[Ni^II(gmma)Cl_2]$ (**1**), $trans-[Ru^II(gmma)Cl_2]$ (**2**) and $[Ru^II(gmma)(PPh_3)Cl]Cl$ (3^+Cl^-) were isolated. The notable observation is that the electro-chemically reduced $trans-[Ni^II(gmma^{\bullet-})Cl_2]^-$ (**1 $^-$**) and $trans-[Ni^II(gmma^{2-})Cl_2]^{2-}$ (**1 $^{2-}$**) ions are not stable in solution and undergo a chemical conversion to a square planar dinuclear nickel(II) complex, predicted as $[(\mu-NSNS-gmma)Ni_2Cl_3(PF_6)]$ (**4 PF_6**), where μ -NSNS-gmma is a

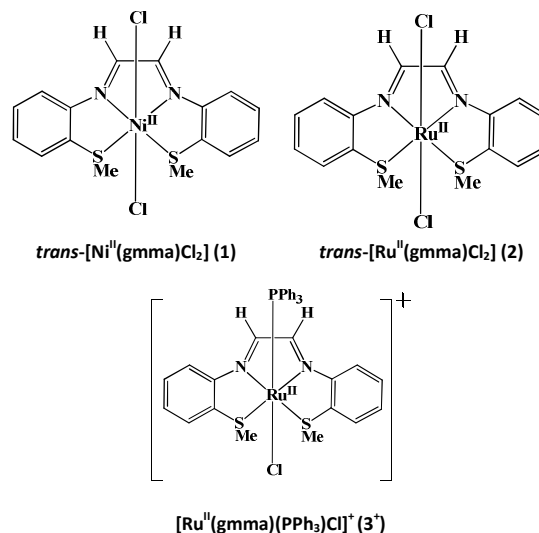


Chart 2 Isolated gmma complexes.

neutral bridging ligand. It is defined as a reduction induced chemical change of an octahedral nickel(II) complex to a square planar complex. In similar condition, the octahedral **2 $^-$** and **3** are stable in solution and these are defined as the resonance hybrids of $[Ru^II(gmma^{\bullet-})] \leftrightarrow [Ru^III(gmma^{2-})]$ states. In this article, syntheses, spectra, electrochemical studies and the single crystal X-ray structures of gmma, **1**.CH₂Cl₂, **2** and **3 $^+Cl^-$** .H₂O are reported. The electrochemically/chemically generated **1 $^-$** , **2 $^-$** and **3** were investigated by EPR spectroscopy and spectroelectrochemical measurements. In addition, density functional theory (DFT) calculations were employed to support in elucidating the electronic structures of the complexes.

Experimental section

Physical measurements

Reagents or analytical grade materials were obtained from the commercial suppliers and used without further purification. Spectroscopic grade solvents were used for spectroscopic and electrochemical measurements. The C, H and N contents of the compounds were obtained from a Perkin-Elmer 2400 Series II elemental analyzer. All analyses were performed after drying the samples under high vacuum. Infrared spectra of the samples were measured from 4000 to 400 cm^{-1} with KBr pellets at room temperature on a Perkin-Elmer Spectrum RX 1 FT-IR spectrophotometer. ¹H and ¹³C NMR spectra in CDCl₃ and DMSO *d*⁶ solvents were obtained on a Bruker DPX 300 and 500 MHz spectrometer. ESI mass spectra were recorded on a micro mass Q-TOF mass spectrometer and Shimadzu LCMS-2020. Electronic absorption spectra in solution at 298 K were obtained on a Perkin-Elmer Lambda 750 spectrophotometer in the range 3300-178 nm. Magnetic susceptibilities at 298 K were measured on a Sherwood Magnetic Susceptibility Balance. The X-band electron paramagnetic resonance (EPR) spectra in a temperature range of 298 to 113 K were measured on a Magnettech GmbH

MiniScope MS400 spectrometer (equipped with temperature controller TC H03), where the microwave frequency was measured with an FC400 frequency counter. The EPR spectra were simulated using EasySpin software package. The electro analytical instrument BASi Epsilon-EC was used for cyclic voltammetric experiments and spectroelectrochemistry measurements.

Materials.

The precursor $[\text{Ru}^{\text{II}}(\text{PPh}_3)_3\text{Cl}_2]$ was prepared by a reported procedure.¹¹

Syntheses. Glyoxalbis(2-mercaptoanil) (gmma). To a 40% aqueous solution of glyoxal (3 mmol), 2-(methylmercapto)aniline (1.12 gm, 8 mmol) was added and mixed well with a glass rod. The mixture turned yellow. To the yellow paste, methanol (15 mL) was added and stirred for 1 h at 310 K. It was filtered and the residue was dried in air and collected. gmma was further re-crystallized in CH_2Cl_2 and EtOH mixture (10:1). Slow evaporation of yellow solution of gmma at 298 K afforded single crystals of gmma, which were collected for X-ray structure analysis. Yield: 0.62 gm (~69% with respect to glyoxal). ESI (positive ion)-MS in CH_3OH ; m/z : 300.03 (gmma). ^1H NMR (CDCl_3 , 500 MHz, 295 K): δ (ppm) = 8.42 (s, 2H), 7.34 (d, 1H), 7.32 (d, 1H), 7.25 (t, 2H), 7.18 (t, 2H), 7.07 (d, 1H), 6.71 (d, 1H), 2.49 (s, 6H). Anal. Calcd. for $\text{C}_{16}\text{H}_{16}\text{N}_2\text{S}_2$ (gmma): C, 63.96; H, 5.37; N, 9.32. Found: C, 63.89; H, 5.28; N, 9.25. IR (KBr, $\nu_{\text{max}}/\text{cm}^{-1}$): 3047 (m; $\nu_{\text{C-H(aromatic)}}$), 2915 (s; $\nu_{\text{C-H(aliphatic)}}$), 1605 (vs, $\nu_{\text{CPh=N}}$), 1571 (s), 1459 (vs), 1437 (vs), 1306 (m), 1276 (m), 1068 (s), 749 (vs), 685 (w).

trans-[Ni^{II}(gmma)Cl₂] (1). To a solution of gmma (301 mg, 1 mmol) in EtOH (30 mL) at 320 K, hydrated NiCl_2 (238 mg, 1 mmol) was added. The mixture was refluxed for 45 min and allowed to cool to room temperature (298 K). Dark-green microcrystals of **1** separated out, which were filtered and the residue were dried in air. Yield: 0.231 gm (~54% with respect to nickel). **1** was further re-crystallized in CH_2Cl_2 . Evaporation of green CH_2Cl_2 solution of **1** under argon afforded single crystals of **1**. CH_2Cl_2 , which were collected for X-ray structure analysis. ESI (positive ion)-MS in CH_3OH ; m/z : 392.91 [**1**-Cl]⁺. Anal. Calcd. for $\text{C}_{16}\text{H}_{16}\text{N}_2\text{S}_2\text{NiCl}_2$ (**1**): C, 44.69; H, 3.75; N, 6.51; Found: C, 44.57; H, 3.68; N, 6.40; IR (KBr, $\nu_{\text{max}}/\text{cm}^{-1}$): 3001 (m, $\nu_{\text{C-H(aromatic)}}$), 2915 (s, $\nu_{\text{C-H(aliphatic)}}$), 1578 (vs, CPh=N-), 1470 (s), 1410 (m), 1378 (s), 942 (m), 917 (m), 760 (vs).

trans-[Ru^{II}(gmma)Cl₂] (2). To a solution of gmma (60 mg, 0.2 mmole) in EtOH (30 mL) at 320 K, $[\text{Ru}^{\text{II}}(\text{PPh}_3)_3\text{Cl}_2]$ (200 mg, 0.2 mmol) was added. The mixture was refluxed for 45 min and allowed to cool to room temperature (298 K). Dark-green microcrystals of **2** separated out, which were filtered and dried in air. Yield: 66 mg (~70% with respect to ruthenium). Single crystals for X-ray structure determination were grown by slow diffusion of *n*-hexane to the dark green CH_2Cl_2 solution of **2**. ESI (positive ion)-MS in CH_3OH ; m/z : 436.87 [**2**-Cl]⁺. ^1H NMR (CDCl_3 , 500 MHz, 295 K): δ (ppm) = 9.28 (s, 1H, CH=N), 8.00 (s, 1H, CH=N), 7.67 (d, 2H), 7.65 (d, 2H), 7.54 (t, 2H), 7.47 (t, 2H), 3.02 (s, 6H). Anal. Calcd. for $\text{C}_{16}\text{H}_{16}\text{N}_2\text{S}_2\text{RuCl}_2$ (**2**): C, 40.68; H, 3.41; N, 5.93; Found: C, 40.56; H, 3.33; N, 5.81; IR (KBr, $\nu_{\text{max}}/\text{cm}^{-1}$): 3066 (s, $\nu_{\text{C-H(aromatic)}}$), 2919 (s, $\nu_{\text{C-H(aliphatic)}}$), 1615 (vs), 1560 (vs, CPh=N-), 1475 (vs), 1418 (vs), 963 (s), 761 (s).

$[\text{Ru}^{\text{II}}(\text{gmma})(\text{PPh}_3)\text{Cl}]\text{Cl}$ (3**⁺Cl⁻).** To a solution of **2** (118 mg, 0.25 mmole) in EtOH (30 mL) at 320 K, PPh_3 (314.4 mg, 1.2 mmol) was added. The mixture was refluxed for 2 h and allowed to cool to room temperature (298 K). Dark-green microcrystals of **3**⁺Cl⁻ separated out, which were filtered and dried in air. **3**⁺Cl⁻ was further purified on a basic alumina column: the unreacted **2** was separated using CH_2Cl_2 as an eluent, while **3**⁺Cl⁻ was collected using a mixture of CH_2Cl_2 and MeOH (20:1) solvents as an eluent. Yield: 72 mg (~40% with respect to **2**). Slow diffusion of *n*-hexane to the dark green solution of **3**⁺Cl⁻ in CH_2Cl_2 with few drops of methanol afforded single crystals for X-ray structure determination. ESI (positive ion)-MS in CH_3OH ; m/z : 699.27 [**3**]⁺. ^1H NMR (CDCl_3 , 300 MHz, 295 K): δ (ppm) = 8.04 (d, 2H), 7.35 (t, 4H), 7.17-7.26 (m, 19H), 2.96 (s, 6H). Anal. Calcd. for $\text{C}_{34}\text{H}_{31}\text{N}_2\text{PS}_2\text{RuCl}$ (**3**⁺Cl⁻): C, 58.40; H, 4.47; N, 4.01; Found: C, 58.33; H, 4.42; N, 3.96; IR (KBr, $\nu_{\text{max}}/\text{cm}^{-1}$): 3059 (vs, $\nu_{\text{C-H(aromatic)}}$), 3050 (s), 2922 (s, $\nu_{\text{C-H(aliphatic)}}$), 1646 (s), 1582 (m, CPh=N-), 1452 (s), 1432 (s), 1270 (s) 1088 (s), 953 (s), 782 (s), 749 (s), 697 (vs, $\nu_{\text{Ru-P(sym)}}$), 530 (vs, $\nu_{\text{Ru-P(asym)}}$).

$[(\mu\text{-NSNS-gmma})\text{Ni}_2\text{Cl}_3(\text{PF}_6)]$ (4**^{PF6}), $[(\mu\text{-NSNS-gmma}^{\text{-}})\text{Ni}_2\text{Cl}_3(\text{PF}_6)]^{\text{-}}$ (**4**^{PF6-}), *trans*- $[\text{Ru}^{\text{III}}(\text{gmma})\text{Cl}_2]^+$ (**2**⁺), *trans*- $[\text{Ru}^{\text{II}}(\text{gmma}^{\text{-}})\text{Cl}_2]^{\text{-}}$ (**2**⁻) and $[\text{Ru}^{\text{II}}(\text{gmma}^{\text{-}})(\text{PPh}_3)\text{Cl}]$ (**3**).** These complexes were not isolated. However, these were generated chemically and electrochemically for spectroelectrochemical measurements, mass and EPR spectra.

X-ray crystallographic data collection and refinement of the structures (CCDC 1497586-1497589)

Single crystals of gmma (yellow), **1**. CH_2Cl_2 (green), **2** (green) and **3**⁺Cl⁻.H₂O (dark green) were picked up with nylon loops and mounted on a Bruker Kappa-CCD and Bruker AXS D8 QUEST ECO diffractometer (at 296 K) diffractometer equipped with a Mo-target rotating anode X-ray source and a graphite monochromator (Mo K α , $\lambda = 0.71073$ Å). Final cell constants were obtained from least-squares fits of all measured reflections. Structures were readily solved by Patterson methods and subsequent difference Fourier techniques. The crystallographic data are given in Table S2. XS. Ver. 2013/1,^{12a} XT. Ver. 2014/4^{12b} and XL. Ver. 2014/7^{12c} were used for the structure solution and refinement. All non-hydrogen atoms were refined anisotropically. Hydrogen atoms were placed at calculated positions and refined as riding atoms with isotropic displacement parameters.

Density functional theory (DFT) and time dependent (TD) DFT calculations

All calculations reported in this article were done with the Gaussian 03W¹³ program package supported by GaussView 4.1. The DFT¹⁴ and TD DFT¹⁵ calculations were performed at the level of a Becke three-parameter hybrid functional with the nonlocal correlation functional of Lee-Yang-Parr (B3LYP).¹⁶ Gas-phase geometries of the ligands and complexes were optimized using Pulay's direct inversion¹⁷ in the iterative subspace (DIIS), "tight" convergent SCF procedure,¹⁸ ignoring symmetry. The gas phase geometries of *trans*- $[\text{Ni}(\text{gmma})\text{Cl}_2]$ (**1**) was optimized with triplet spin state. The spin states used for the optimizations of other species are: singlet for gmma, *trans*- $[\text{Ru}(\text{gmma})\text{Cl}_2]$ (**2**), $[\text{Ru}^{\text{II}}(\text{gmma})(\text{PMe}_3)\text{Cl}]^+$ (**3**^{Me+}) and

ARTICLE

Journal Name

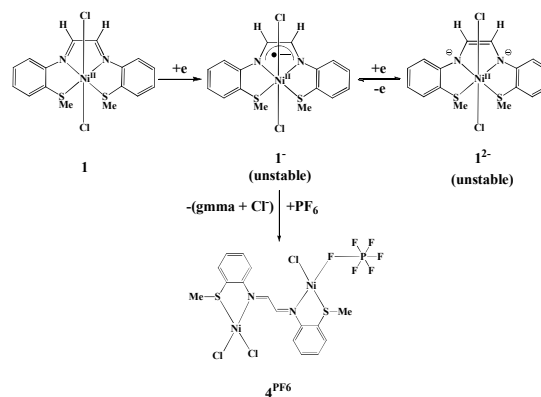
trans-[Ni(gmma)Cl₂]²⁻ (**1**²⁻); doublet for *trans*-[Ni(gmma)Cl₂]⁻ (**1**⁻), *trans*-[Ru(gmma)Cl₂]⁻ (**2**⁻), *trans*-[Ru(gmma)Cl₂]⁺ (**2**⁺) and [Ru^{II}(gmma)(PMe₃)Cl] (**3**^{Me+}). In all calculations, a LANL2DZ basis set along with the corresponding effective core potential (ECP) was used for nickel, zinc and ruthenium metals.¹⁹⁻²¹ The valence double- ζ basis set 6-31G²² for H was used. For the non-hydrogen atoms C, N, O, P, S and Cl, valence double- ζ with diffuse and polarization functions, 6-31+G*²³ as basis set was employed for all calculations. The percentage contributions of metal, chloride, gmma and gmha ligands to the frontier orbitals were calculated using the GaussSum program package.²⁴ The 60 lowest singlet excitation energies on each of the optimized geometries of gmma, **1**, **2** and **3**^{Me+} were calculated by the TD DFT method.²⁵ The natures of transitions were calculated by adding the probability of the same type among α and β molecular orbitals.

Results and discussion

Syntheses

The α -diimine ligand, glyoxalbis(2-methylmercaptoanil) (gmma) and the coordination complexes of it reported in this article are summarized in Chart 2. Details of the syntheses are outlined in the experimental section. Towards nickel(II) ion gmma is a flexidentate ligand exhibiting two types of binding modes: tetradentate N₂S₂-donor as gmma and bis(methylthioimine) donor bridging ligand¹⁰ abbreviated as μ -NSNS-gmma. Reaction of gmma with NiCl₂·xH₂O afforded **1**. **2** was isolated from a reaction of [Ru^{II}(PPh₃)₃Cl₂] with gmma in boiling ethanol. Reaction of **2** with excess triphenyl phosphine in boiling ethanol afforded **3**⁺.

Notably, the reduced **1**⁻ and **1**²⁻ ions in solution are unstable and the octahedral complex ions convert to a square planar dinuclear nickel(II) complex. The chemical conversion of **1**⁻ and **1**²⁻ ions was investigated by ESI mass spectroscopy. The constant potential coulometric reductions of **1** → **1**⁻ and **1** → **1**²⁻ (respectively at -0.5 V and -0.9 V vs Fc^{+/0}/Fc couple, *vide infra*) in CH₂Cl₂ using tetrabutylammonium hexafluorophosphate as electrolyte were performed. In both cases the yellowish green solutions of the reduced complexes in air turned brown due to the formation of **4**^{PF₆} as depicted in Scheme 2. Analyses of these solutions by ESI mass spectra reveal the m/z peaks at 520 and 630 corresponding to [Ni₂(gmma)Cl₃]⁺ and [Ni₂(gmma)Cl₂(PF₆)]⁺ molecular ions as illustrated in Fig. S2(a). During the chromatographic separation, **4**^{PF₆} decomposes and isolation of pure **4**^{PF₆} did not succeed. However, the brown coating on the platinum working electrode obtained during electrolysis was the pure **4**^{PF₆} authenticated by the ESI mass spectroscopy (see, Fig. S2(b)). Chemical reduction of **1** also results in the formation of the [Ni₂(gmma)Cl₃]⁺. The green CH₂Cl₂ solution of **1** on addition of two equivalent of cobaltocene turned immediately brown that gave the m/z peak only due to [Ni₂(gmma)Cl₃]⁺. However the ESI mass spectrum of the solution obtained after the chemical reduction of **1** by cobaltocene in presence of

Scheme 2 Reduction induced chemical change of **1**.

tetrabutylammonium hexafluorophosphate displayed m/z peaks due to **4**^{PF₆} (major).

Molecular geometries

Single crystal X-ray structure determinations confirmed the tetradentate N₂S₂-binding mode of gmma in **1**·CH₂Cl₂, **2** and **3**⁺·Cl⁻·H₂O. To compare the bond parameters of the diimine fragments of the complexes, single crystal X-ray structure of gmma was also determined. The crystallographic data are summarized in Table S1. The significant bond parameters are summarized in Table 1. The ligand, gmma crystallizes in the P2₁/n space group and it exhibits trans geometry (Fig. S3). The average C=N and NC-CN lengths of gmma are 1.212(3) and 1.436(4) Å.

1·CH₂Cl₂ crystallizes in the *Pnma* space group. The molecular structure in the crystals and the atom labeling scheme are illustrated in Fig. 1(a). The gmma ligand with nickel(II) ion, excluding the two methyl substituents which are cis to each other, is approximately planar and the two Cl ligands reside trans to each other. The average Ni(1)-N_{imine} and Ni(1)-S(1) distances are 2.030(2) and 2.436(1) Å. The average Ni^{II}-Cl lengths are 2.395(1) Å. These lengths correlate well to those reported in the similar types of diimine complexes of nickel(II) ion.⁶ The average C=N lengths, 1.282(2) Å, are relatively longer. However, these bond parameters are quite consistent to the coordination of neutral gmma ligand to nickel(II) ion.

2 crystallizes in the P2₁/c space group and iso-structural to **1**·CH₂Cl₂. The molecular geometry in the crystals and the atom labeling scheme are shown in Fig. 1(b). The average Ru^{II}-N_{imine} and Ru^{II}-SME lengths are 1.981(3) and 2.367(2) Å. The extent of deformation of the α -diimine fragment of **2** is relatively larger. The average C=N lengths are 1.321(5) Å, while, the NC-CN length is 1.401(7) Å as listed in Table 1. The similar features of the bond parameters were established in other α -diimine complexes of ruthenium(II).^{26,27} Thus, **2** is defined as a neutral gmma complex of ruthenium(II) ion as defined by the **2**^{Ru(II)L} state of Chart 3. The relatively longer C=N and shorter NC-CN lengths of **2** can be explained by a resonance contribution of the di-radical state, **2**^{Ru(III)L•+} as depicted in Chart 3, to the ground electronic state of **2**.

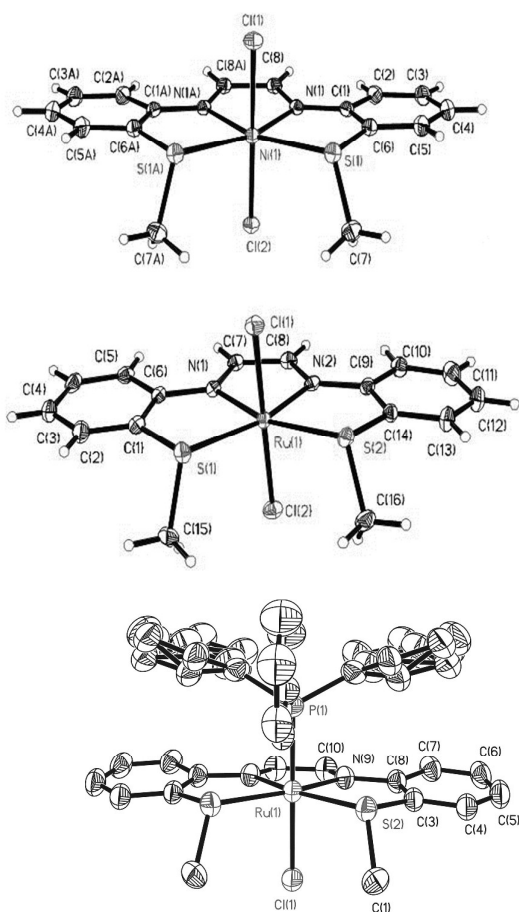


Fig. 1 Molecular geometries of (a) $1 \cdot \text{CH}_2\text{Cl}_2$, (b) 2 and (c) $3^+\text{Cl}^- \cdot \text{H}_2\text{O}$ in crystals (40% thermal ellipsoids; solvents and anion are omitted for clarity).

The molecular geometry of $3^+\text{Cl}^- \cdot \text{H}_2\text{O}$ that crystallizes in the $P6(3)/m$ space group, and the atom labeling scheme are shown in Fig. 1(c). A split model is used to refine the disordered phenyl rings and PLATON/SQUEEZE is used to remove disordered solvent from a solvent channel (see ESI[†]). The approximate geometry of 3^+ ion that incorporates a PPh_3 ligand, is similar to that of 2 . The bond parameters of the coordination sphere reflect the effect of the coordination of

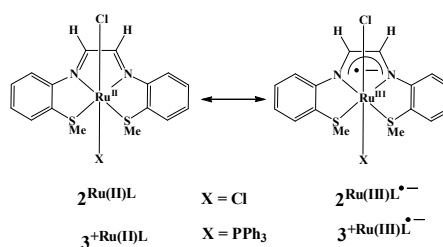


Chart 3 Two possible descriptions of the (one and only) electronic state

the π -acidic PPh_3 ligand to 3^+ ion. Due to stronger $d_{\text{Ru}} \rightarrow \text{PPh}_3$ back bonding, $d_{\text{Ru}} \rightarrow \pi^*$ back bonding is less effective in 3^+ ion. Consequently, the average $\text{Ru}^{\text{II}}-\text{N}_{\text{imine}}$ lengths, 2.008(3) Å of 3^+ ion are relatively longer than those found in 2 (see Table 1). The diimine fragment of 3^+ is relatively less deformed inferring the smaller contribution of $3^{+\text{Ru(III)L}^{+}}$ state to the ground electronic state of 3^+ ion. The average C=N and NC-CN lengths are 1.303(5) and 1.432(9) Å.

Redox activities

The redox activities of gmma , 1 , 2 and 3^+ were investigated by cyclic voltammetry in CH_2Cl_2 at 298 K. The redox potential data referenced to ferrocenium/ferrocene (Fc^+/Fc) couple are summarized in Table S2. It is observed that both cathodic and anodic waves due to $\text{gmma}/\text{gmma}^{+}$ and $\text{gmma}^+/\text{gmma}$ redox couples are irreversible as shown in Fig. 2(a). However, the cathodic wave due to $\text{gmma}/\text{gmma}^{+}$ redox couple in complexes is reversible. 1 exhibits two cathodic waves at -0.34 V (peak-to-peak separation, 260 mV) and -0.59 V (peak-to-peak separation, 90 mV). The former wave is assigned to $[\text{Ni}^{\text{II}}(\text{gmma})]/[\text{Ni}^{\text{II}}(\text{gmma}^{+})]^-$ (1^-) redox couple, while the latter is assigned to $[\text{Ni}^{\text{II}}(\text{gmma}^{+})]/[\text{Ni}^{\text{II}}(\text{gmma}^{2+})]^{2-}$ (1^{2-}). The EPR and ESI mass spectra of the reduced species authenticated that 1^- and 1^{2-} ions are not stable in solution and undergo a chemical change to 4^{PF_6} . The instability of the 1^- and 1^{2-} ions makes the first redox wave ($E_{1/2}^1$) due to the $\text{gmma}/\text{gmma}^{+}$ redox couple, irreversible ($i_c/i_a = 1.19$) as shown in Fig. 2(b). However, the second cathodic wave ($E_{1/2}^2$) due to $\text{gmma}^+/\text{gmma}^{2+}$ redox couple in the experimental scan-period is reversible ($i_c/i_a = 1.0$). The redox activity of dinuclear species is different from that of 1 . The $\mu\text{-NSNS-gmma}/\mu\text{-NSNS-gmma}^{+}$ redox couple of 4^{PF_6} at -1.28 is reversible ($i_c/i_a = 1.0$) as depicted in Fig. 2(c).

Table 1 Selected experimental bond lengths (Å) of gmma , $1 \cdot \text{CH}_2\text{Cl}_2$, 2 and $3^+\text{Cl}^- \cdot \text{H}_2\text{O}$ and the corresponding calculated bond parameters of 1 , 2 , 2^- , $3^{\text{Me}+}$, 3^{Me} and $3^{\text{Me}-}$ obtained from the B3LYP/DFT calculations

Bond Types	1			2			3 ⁺					
	gmma (exptl)	1·CH ₂ Cl ₂ (exptl)	1 (calcd)	1 ⁻ (calcd)	1 ²⁻ (calcd)	2 (exptl)	2 (calcd)	2 ⁻ (calcd)	3 ⁺ Cl ⁻ ·H ₂ O (exptl)	3 ^{Me+} (calcd)	3 ^{Me} (calcd)	3 ^{Me-} (calcd)
avg M-N _{imine}	-	2.030(2)	2.084	2.062	1.937	1.981(3)	2.001	2.026	2.008(3)	2.024	2.049	2.062
avg M-SMe	-	2.436(1)	2.527	2.597	2.270	2.367(2)	2.445	2.439	2.357(2)	2.449	2.439	2.448
avg M-Cl	-	2.395(1)	2.405	2.452	2.328	2.391(2)	2.443	2.490	2.461(2)	2.465	2.520	2.583
M-PPh ₃	-	-	-	-	-	-	-	-	2.320(2)	2.395	2.340	2.295
avg C=N	1.212(3)	1.282(2)	1.291	1.333	1.395	1.321(5)	1.327	1.359	1.303(5)	1.320	1.351	1.385
NC-CN	1.436(4)	1.460(3)	1.457	1.406	1.379	1.401(7)	1.415	1.385	1.432(9)	1.426	1.394	1.349

ARTICLE

Both anodic and cathodic waves of **2** at +0.48 V due to $[\text{Ru}^{\text{III}}(\text{gmma})]/[\text{Ru}^{\text{II}}(\text{gmma})]$ redox couple ($i_c/i_a = 1.0$) and -1.18 V due to $[\text{Ru}^{\text{II}}(\text{gmma})]/[\text{Ru}^{\text{II}}(\text{gmma}^{\cdot-})]$ redox couple ($i_c/i_a = 1.0$) are reversible as illustrated in Fig. 3(a). The similar anodic wave is absent in **1** as the corresponding nickel(III) state is hard to achieve with the softer gmma ligand. $\mathbf{3}^+$ ion exhibits two cathodic waves at -0.73 and -1.36 V. The first one is reversible ($i_c/i_a = 1.0$), while the second wave is irreversible ($i_c/i_a = 1.5$) as illustrated in Fig. 3(b). The potential data implies that $\mathbf{3}^+$ is easily reducible than **2**. The second reduction of $\mathbf{3}^+$ ion due to $\text{gmma}^{\cdot-}/\text{gmma}^{2-}$ redox couple, is not observable in case of **2**. It is the effect of introducing π -acidic PPh_3 ligand to $\mathbf{3}^+$ ion. Notably, the anodic wave due to $[\text{Ru}^{\text{III}}(\text{gmma})]/[\text{Ru}^{\text{II}}(\text{gmma})]$ couple of $\mathbf{3}^+$ ion is completely irreversible.

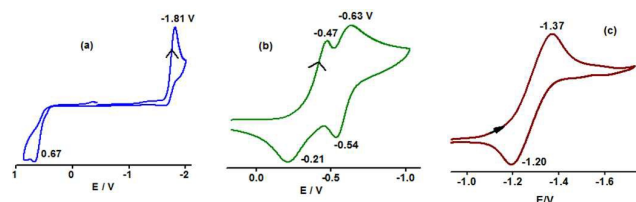


Fig. 2 Cyclic voltammograms of (a) gmma, (b) **1** and (c) $\mathbf{4}^{\text{PF}_6}$ in CH_2Cl_2 at 298 K. Conditions: 0.20 M $[\text{N}(\text{n-Bu})_4]\text{PF}_6$ supporting electrolyte; platinum working electrode; scan rate 100 mVs^{-1} .

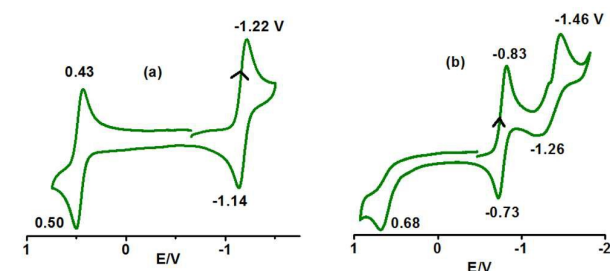


Fig. 3 Cyclic voltammograms of (a) **2** and (b) $\mathbf{3}^+\text{Cl}^-$ in CH_2Cl_2 at 298 K. Conditions: 0.20 M $[\text{N}(\text{n-Bu})_4]\text{PF}_6$ supporting electrolyte; platinum working electrode (Scan rate 100 mVs^{-1}).

EPR spectroscopy

Magnetic susceptibility measurements at 298 K confirmed the paramagnetism of **1** ($\mu_{\text{eff}} = 2.85$). The parameters of the EPR measurements are listed in Table S3 and the simulated g values and the coupling constants are summarized in Table 2. In the X-band EPR spectrum no signal of **1** was detected, due to large zero field splitting.²⁸ However, $\mathbf{1}^-$ ion obtained after reduction of **1** by cobaltocene in CH_2Cl_2 , exhibits an isotropic EPR signal due to $S_t = \frac{1}{2}$ state at $g = 2.184$ as illustrated in Fig. 4(a). The frozen glass spectrum displays a rhombic signal at $g_1 = 2.230$, $g_2 = 2.185$ and $g_3 = 2.089$ as shown in Fig. 4(b), which corroborate well to those of the nickel(I) complexes.⁶ The $S_t = \frac{1}{2}$ spin state of $\mathbf{1}^-$ can be achieved either by reduction of nickel(II) ion or by reduction of gmma to $\text{gmma}^{\cdot-}$ that couples to $S_t = 1$ state of an octahedral nickel(II) ion. In case of **1** reduction occurs at the diimine fragment converting gmma to $\text{gmma}^{\cdot-}$. The anion radical couples anti-ferromagnetically to one of the electrons of the nickel(II) ion (*vide infra*) producing

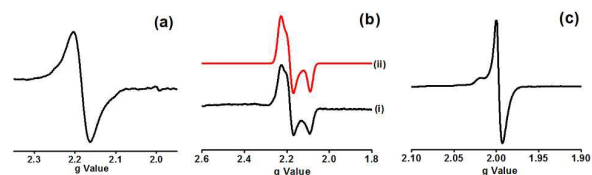


Fig. 4 X-band EPR spectra of $\mathbf{1}^-$ ion (a) CH_2Cl_2 solution (298 K) and (b) CH_2Cl_2 frozen glass (113 K) ((i) experimental (black), (ii) simulated (red)); (c) chemically generated $\mathbf{4}^{\text{PF}_6-}$ at 113 K.

a metal centred $S_t = \frac{1}{2}$ state and exhibits an anisotropic EPR spectrum. However, the EPR spectrum of $\mathbf{4}^{\text{PF}_6-}$ ion achieved by reduction of the crude product $\mathbf{4}^{\text{PF}_6}$ with excess cobaltocene in CH_2Cl_2 reveals a signal at $g = 1.997$ as depicted Fig. 4(c). It is analyzed that the $\mathbf{4}^{\text{PF}_6-}$ ion is a square planar nickel(II) complex of $\text{gmma}^{\cdot-}$.

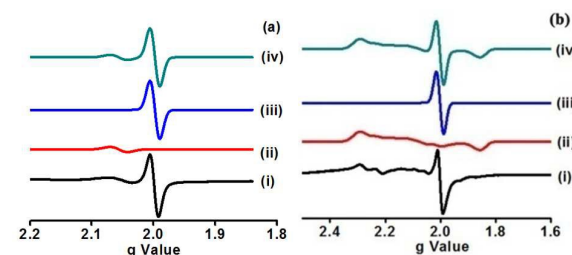


Fig. 5 X-band EPR spectra of $\mathbf{2}^-$ (a) CH_2Cl_2 solution (298 K) (i) black, experimental spectrum; (ii) red, simulated spectrum considering the $\text{trans-}[\text{Ru}^{\text{II}}(\text{gmma}^{2-})\text{Cl}_2]^-$ state; (iii) blue, simulated spectrum considering the $\text{trans-}[\text{Ru}^{\text{II}}(\text{gmma}^{\cdot-})\text{Cl}_2]^-$ state; (iv) green, simulated spectrum considering the $\text{trans-}[\text{Ru}^{\text{II}}(\text{gmma}^{\cdot-})\text{Cl}_2]^-$ canonical structures and (b) CH_2Cl_2 frozen glass (113 K) (i) black, experimental spectrum; (ii) red, simulated spectrum considering the $\text{trans-}[\text{Ru}^{\text{II}}(\text{gmma}^{2-})\text{Cl}_2]^-$ state; (iii) blue, simulated spectrum considering the $\text{trans-}[\text{Ru}^{\text{II}}(\text{gmma}^{\cdot-})\text{Cl}_2]^-$ state; (iv) green, simulated spectrum considering the $\text{trans-}[\text{Ru}^{\text{II}}(\text{gmma}^{\cdot-})\text{Cl}_2]^-$ and $\text{trans-}[\text{Ru}^{\text{II}}(\text{gmma}^{2-})\text{Cl}_2]^-$ canonical structures.

The EPR spectra of the chemically reduced $\mathbf{2}^-$ ion recorded at different temperature (298-113 K) are shown in Fig. S4. The fluid solution and the frozen glass spectra with simulations are depicted in Fig. 5. It is noted that in addition to an isotropic signal due to $\text{trans-}[\text{Ru}^{\text{II}}(\text{gmma}^{\cdot-})\text{Cl}_2]^-$ state at $g = 2.000$, the fluid solution EPR spectrum of $\mathbf{2}^-$ ion contains another signal at $g = 2.059$. In frozen glass the anisotropic component gives a rhombic signal at $g_1 = 2.180$, $g_2 = 2.130$ and $g_3 = 1.860$. The frozen glass EPR spectrum of $\mathbf{2}^-$ ion was simulated considering $\text{trans-}[\text{Ru}^{\text{II}}(\text{gmma}^{\cdot-})\text{Cl}_2]^-$ and $\text{trans-}[\text{Ru}^{\text{II}}(\text{gmma}^{2-})\text{Cl}_2]^-$ canonical states. The anisotropic signal is reproducible both chemically/electrochemically, eliminating the possibility of the existence of the paramagnetic impurity. The spectra are similar in presence of tetrabutylammonium chloride precluding the chloride dissociation. It infers that in $\mathbf{2}^-$ ion the spin is shared by both ruthenium and gmma ligand.

The g -anisotropy (Δg) of the frozen glass is 0.32 which is relatively larger than those observed in organic radicals.^{6,9,26,27} However, the Δg value correlates well to that observed in the ruthenium(III) complexes.^{26,27} Thus the $\mathbf{2}^-$ is defined as a resonance hybrid of $\text{trans-}[\text{Ru}^{\text{II}}(\text{gmma}^{\cdot-})\text{Cl}_2]^-$ and $\text{trans-}[\text{Ru}^{\text{II}}(\text{gmma}^{2-})\text{Cl}_2]^-$ states, the latter state is responsible for the

Table 2 X-Band EPR spectral parameters of **1**⁻, **2**⁻, **2**⁺, **3** and **4**^{PF6-}

Complexes	$g_1/g_2/g_3$	g_{iso}/g_{av}	$^a\Delta g$
1 ⁻			
CH ₂ Cl ₂ solution (298 K)		2.184	0
CH ₂ Cl ₂ frozen glass (113 K)	2.230/2.185/2.089	2.168	0.14
2 ⁻			
CH ₂ Cl ₂ solution (298 K)			
contribution of ^c cs:			
<i>trans</i> -[Ru ^{II} (<i>gmma</i> ⁻)Cl ₂] ⁻		1.998	0
<i>trans</i> -[Ru ^{III} (<i>gmma</i> ²⁻)Cl ₂] ⁻		2.059	0
CH ₂ Cl ₂ frozen glass (113 K)			
contribution of ^c cs:			
<i>trans</i> -[Ru ^{II} (<i>gmma</i> ⁻)Cl ₂] ⁻		2.002	
<i>trans</i> -[Ru ^{III} (<i>gmma</i> ²⁻)Cl ₂] ⁻	2.180/2.130/1.860 (^b A= 53/76/13 G)	2.056	0.32
2 ⁺			
CH ₂ Cl ₂ frozen glass (113 K)	2.165/2.089/1.968 (A= 36/10/36 G)	2.074	0.20
3			
CH ₂ Cl ₂ solution (298 K)			
contribution of ^c cs:			
[Ru ^{II} (<i>gmma</i> ⁻)(PPh ₃)Cl]		2.005	0
[Ru ^{III} (<i>gmma</i> ²⁻)(PPh ₃)Cl]		2.068	0
CH ₂ Cl ₂ frozen glass (113 K)			
contribution of ^c cs:			
[Ru ^{II} (<i>gmma</i> ⁻)(PPh ₃)Cl]		2.005	
[Ru ^{III} (<i>gmma</i> ²⁻)(PPh ₃)Cl]	2.126/1.995/1.905 (A=17/9/17 G)	2.009	0.22
4 ^{PF6-}			
		1.997	0

^a $\Delta g = g_{max} - g_{min}$; ^bA is due to ^{99,101}Ru = 5/2 nucleus; ^ccs = canonical states

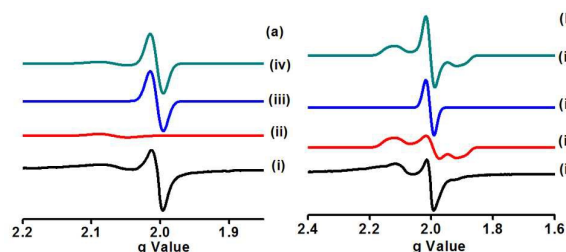


Fig. 6 X-band EPR spectra of **3** (a) CH₂Cl₂ solution at 298 K, (i) black, experimental spectrum; (ii) red, simulated spectrum considering the [Ru^{III}(*gmma*²⁻)(PPh₃)Cl] state; (iii) blue, simulated spectrum considering the [Ru^{II}(*gmma*⁻)(PPh₃)Cl] state; (iv) green, simulated spectrum considering [Ru^{III}(*gmma*²⁻)(PPh₃)Cl] and [Ru^{II}(*gmma*⁻)(PPh₃)Cl] canonical structures. (b) CH₂Cl₂ frozen glass at 113 K, (i) black, experimental spectrum; (ii) red, simulated spectrum considering the [Ru^{III}(*gmma*²⁻)(PPh₃)Cl] state; (iii) blue, simulated spectrum considering the [Ru^{II}(*gmma*⁻)(PPh₃)Cl] state; (iv) green, simulated spectrum considering the [Ru^{III}(*gmma*²⁻)(PPh₃)Cl] and [Ru^{II}(*gmma*⁻)(PPh₃)Cl] canonical structures.

anisotropy of the spectrum. The X-ray bond parameters of the diimine fragment also suggested a contribution of ruthenium(III) state to **2**. The CH₂Cl₂ frozen glass EPR spectrum of **2**⁺ is anisotropic as illustrated in Fig. S5. The simulated *g* parameters as listed in Table 2, are similar to those reported in cases of ruthenium(III) complexes incorporating redox non-innocent diimine fragments.^{26,27} It infers that **2**⁺ ion is a ruthenium(III) complex of the type *trans*-[Ru^{III}(*gmma*)Cl₂]⁺.

The X-band EPR spectra of **3** (CH₂Cl₂ solution and frozen glass) at different temperature (298-113 K) are illustrated in Fig. S6. The spectra are similar to that of **2**⁻ ion. Both solution and frozen glass EPR spectra of **3** were simulated considering [Ru^{II}(*gmma*⁻)] and [Ru^{III}(*gmma*²⁻)] canonical states as illustrated in Fig. 6(a) and Fig. 6(b). However, the Δg value in case of **3** is relatively small ($g_1 = 2.126$, $g_2 = 1.995$ and $g_3 = 1.905$, $\Delta g = 0.22$), predicting a smaller contribution of [Ru^{III}(*gmma*²⁻)] state to **3** in comparison to that in **2**⁻ ion. It is the effect of introduction of π acidic PPh₃ ligand to **3**.

Density functional theory (DFT) calculations and the electronic structures of the complexes

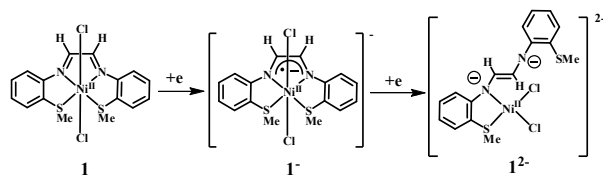
In conjunction with the X-ray bond parameters and EPR spectroscopy, DFT calculations at the B3LYP level of the theory were used to elucidate the electronic structures of **1**, **2** and **3**⁺.

gmma, **gmma**⁻ and [Zn^{II}(*gmma*)Cl₂]. To analyze the geometrical features and the bond parameters of the ligand, the gas phase geometries of the neutral (*E* form with singlet spin state) and one electron reduced (doublet spin state) *gmma* were optimized. The calculated C=N lengths of *gmma* and *gmma*⁻ are 1.285 and 1.333 Å. The NC-CN lengths of *gmma* and *gmma*⁻ are 1.458 and 1.405 Å. In the reduced analogue the atomic spin is dominantly localized on the imine function inferring the formation of a π -anion radical, abbreviated as *gmma*⁻ as depicted in Fig. S7. The bond parameters of the coordinated *Z* form were calculated optimizing [Zn^{II}(*gmma*)Cl₂] complex with singlet spin state. The calculated C=N and NC-CN lengths of the coordinated *Z* form are 1.289 and 1.461 Å.

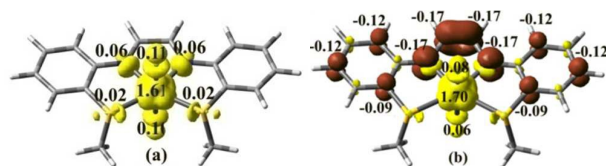
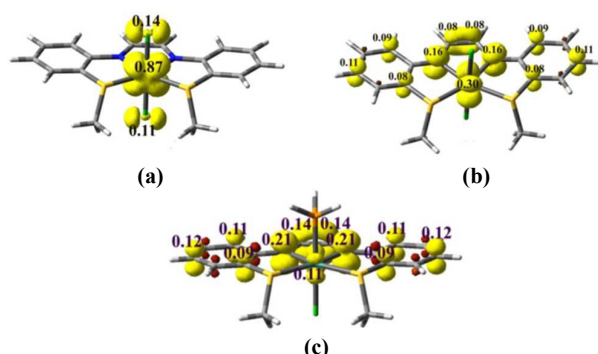
trans-[Ni^{II}(*gmma*)Cl₂] (**1**), *trans*-[Ni^{II}(*gmma*⁻)Cl₂]⁻ (**1**⁻) and *cis*-[Ni^{II}(*gmma*²⁻)Cl₂]²⁻ (**1**²⁻). Gas phase geometries of **1**, **1**⁻ and **1**²⁻ were optimized respectively with the triplet, doublet and singlet spin states. The calculated bond parameters of **1** correlate well to those obtained from the single crystal X-ray structure determination of **1**.CH₂Cl₂ (see Table 1). It is to be noted that the calculated bond parameters of the coordinated diimine fragment of these three species are significantly different. In **1**, the calculated average C=N and NC-CN lengths are 1.291 and 1.457 Å which are similar to those observed in the optimized geometry of the *gmma* ligand and [Zn^{II}(*gmma*)Cl₂]. It infers the coordination of the neutral *gmma* ligand to nickel(II) ion in **1**. The atomic spin of **1** is shown in Fig. 7(a). On the contrary, the calculated C=N length of **1**⁻ ion, 1.333 Å, is relatively longer, while the NC-CN length, 1.406 Å, is relatively shorter. The trend is consistent with those of diimine anion radicals coordinated to the transition metal ions.^{6,26,27} It establishes that in **1**⁻, *gmma* ligand is reduced to *gmma*⁻ which results the anti-ferromagnetic coupling to nickel(II) ion affording a $S_t = \frac{1}{2}$ spin state. The atomic spin obtained from the Mulliken spin population analysis, disperses on *gmma* as shown in Fig. 7(b), corroborating to the formation of *gmma*⁻, coordinated to the nickel(II) ion. Thus, **1**⁻ ion is defined as a octahedral *gmma*⁻ complex of nickel(II) ion of the type *trans*-[Ni^{II}(*gmma*⁻)Cl₂]⁻. The calculated bond parameters and the

ARTICLE

Journal Name



Scheme 3

Fig. 7 Atomic spin of (a) **1** and (b) **1**⁺ (isovalue = 0.004).Fig. 8 Atomic spin of (a) **2**⁺, (b) **2**⁻ and (c) **3**^{Me} (isovalue = 0.004).

molecular geometry of the singlet **1**²⁻ ion are surprisingly different from those of the octahedral geometries of the paramagnetic **1** and **1**⁺ ion. The closed shell singlet (CSS) solution converged to a square planar nickel(II) complex as shown in Chart S1(a). The optimized geometry is illustrated in Chart S1(a). The calculated C=N lengths are 1.395 and 1.359 Å, while the NC-CN length is 1.379 Å. The calculation infers that the dianionic gmma²⁻ coordinates the nickel(II) ion as a NS-donor bidentate ligand. For comparison, the square planar geometry of **1**²⁻ with NN-chelate (see Chart S1(b)) was also optimized with singlet spin state. However, the square planar complex with NS-chelate is 1.87 kJ/mole, lower in energy than that the NN-chelate. The DFT calculations reveal that octahedral **1**²⁻ ion is not stable and undergoes geometrical reorganization, which is the origin of the irreversibility of the first cathodic redox wave of **1**.

trans-[Ru^{II}(gmma)Cl₂] (**2**), **trans**-[Ru^{III}(gmma)Cl₂]⁺ (**2**⁺) and **trans**-[Ru^{II}(gmma^{•-})Cl₂]⁻ ↔ **trans**-[Ru^{III}(gmma²⁻)Cl₂]⁻ (**2**⁻). Gas phase geometries of **2**, **2**⁺ and **2**⁻ ions were optimized respectively with singlet, doublet and doublet spin states. As both metal ion and the coordinated gmma ligand are redox non-innocent, the ground electronic state of **2** can be defined by the resonance structures of CSS (**2**^{Ru(II)L}) and the diradical open shell singlet (**2**^{Ru(III)L••}) states as illustrated in Chart 3. The bond parameters of these two electronic states of the diimine fragment are significantly different. In **2**, the calculated C=N

and NC-CN lengths of the diimine fragment are 1.327 and 1.415 Å (see Table 1). However, the CSS solution of **2** is stable and no instability due to open shell singlet (OSS) perturbation was recorded, discarding the possibility of **2**^{Ru(III)L••} as a ground state. Analyses of molecular orbitals of **2** affirmed the mixing of the π* orbital with the ruthenium d-orbitals as depicted in Figure S8, resulting in a delocalization of the t_{2g}⁶ electrons to the diimine fragment. The feature promotes **2**^{Ru(III)L••} state to contribute to **2**. The experimental and calculated bond parameters of the diimine fragment suggest a mixing of **2**^{Ru(II)L} and **2**^{Ru(III)L••} states in **2**.²⁹ The features are similar to those observed in the diimine and osazone complexes of ruthenium(II) reported recently.²⁶ The shorter average C=N lengths, 1.317 Å, and the localization of atomic spin on ruthenium as illustrated in Fig. 8(a) confirmed that the paramagnetic **2**⁺ ion is a ruthenium(III) complex of the type **trans**-[Ru^{III}(gmma)Cl₂]⁺. The calculated bond parameters of the diimine fragment and the coordination sphere of **2**⁻ ion are notably different from those of **2** and **2**⁺ ion.

The average C=N lengths of the diimine fragment of **2**⁻ ion is 1.359 Å which is relatively longer than those of [Zn^{II}(gmma)Cl₂] and **2**⁺ ion. The NC-CN length is relatively shorter, 1.385 Å. The trend corroborates well to those observed in gmma^{•-} and diimine anion radical complexes of transition metal ions.^{5,6,8,9} The atomic spin obtained from the Mulliken spin population analysis, as shown in Fig. 8(b), is consistent to the existence of gmma^{•-} in **2**⁻ ion. However, a significant amount of spin (~30%) shared by one of the t_{2g} orbitals of the ruthenium ion, infers a contribution of the **trans**-[Ru^{III}(gmma²⁻)Cl₂]⁻ state to **2**⁻ ion. The contribution of **trans**-[Ru^{III}(PQ^{•-})(PPh₃)₂Cl₂]⁻ and **trans**-[Ru^{II}(PQ^{•-})(PPh₃)₂Cl₂]⁻ states similarly was assigned to the reduced species of the 9,10-phenanthrenesemiquinonate anion radical (PQ^{•-}) complexes of ruthenium(III) of the type **trans**-[Ru^{III}(PQ^{•-})(PPh₃)₂Cl₂].³⁰ Thus, the ground electronic state of **2** ion is defined as a resonance hybrid of **trans**-[Ru^{II}(gmma^{•-})Cl₂]⁻ and **trans**-[Ru^{III}(gmma²⁻)Cl₂]⁻ states. No contribution of the ruthenium(I) state is predicted in these chemical systems.³¹

[Ru^{II}(gmma)(PPh₃)Cl]⁺ (**3**⁺), [Ru^{II}(gmma^{•-})(PPh₃)Cl] ↔ [Ru^{III}(gmma²⁻)(PPh₃)Cl] (**3**) and [Ru^{II}(gmma²⁻)(PPh₃)Cl]⁻ (**3**⁻)
The calculated C=N and NC-CN lengths of the diimine fragments of [Ru^{II}(gmma)(PMe₃)Cl]⁺ (**3**^{Me+}), [Ru^{II}(gmma)(PMe₃)Cl] (**3**^{Me}) and [Ru^{II}(gmma)(PMe₃)Cl]⁻ (**3**^{Me-}), optimized with singlet, doublet and singlet spin states are significantly different (see Table 1). In **3**^{Me+} → **3**^{Me} → **3**^{Me-} conversions, the C=N lengths gradually increase, while NC-CN lengths decrease as: C=N, (**3**^{Me+}, 1.320; **3**^{Me}, 1.351; **3**^{Me-}, 1.385 Å) and NC-CN (**3**^{Me+}, 1.426; **3**^{Me}, 1.394; **3**^{Me-}, 1.349 Å). The CSS solution of **3**^{Me+} ion is also stable inferring that **3**⁺ ion is a ruthenium(II) complex of neutral gmma ligand. Similar to **2**⁻ ion, atomic spin of **3**^{Me} scatter on the both diimine fragment and the ruthenium (~11%) as illustrated in Fig. 8(c). Thus **3** is also defined as a resonance hybrid of [Ru^{II}(gmma^{•-})(PPh₃)Cl] and [Ru^{III}(gmma²⁻)(PPh₃)Cl] states. In comparison to **2**⁻ ion, the atomic spin on ruthenium in **3** is relatively smaller, predicting a lower stability of the ruthenium(III) state with PPh₃ as a co-ligand. The bond parameters of the gmma ligand of the **3**^{Me-}

correspond to those of the diimide state (C=N, 1.385 Å, Table 1) and it is defined as a gmma^{2-} complex of ruthenium(II) of the type $[\text{Ru}^{\text{II}}(\text{gmma}^{2-})(\text{PPh}_3)\text{Cl}]^-$.

Electronic spectra, spectroelectrochemical measurements and time dependent (TD) DFT calculations

The UV-vis absorption spectra of gmma , **1**, **2** and $\mathbf{3}^+\text{Cl}^-$ were recorded in CH_2Cl_2 at 298 K. The spectra are shown in Fig. 9 and the spectral data are summarized in Table 3. A qualitative absorption spectrum of $\mathbf{4}^{\text{PF}_6}$ is depicted in Fig. S2. The origins of the absorption bands were elucidated by the TD DFT calculations on gmma , **1**, **2** and $\mathbf{3}^{\text{Me}^+}$ in CH_2Cl_2 using CPCM model with the singlet spin state. The excitation energies with the oscillator strengths and the transition types are also summarized in Table S4. The absorption spectrum of gmma

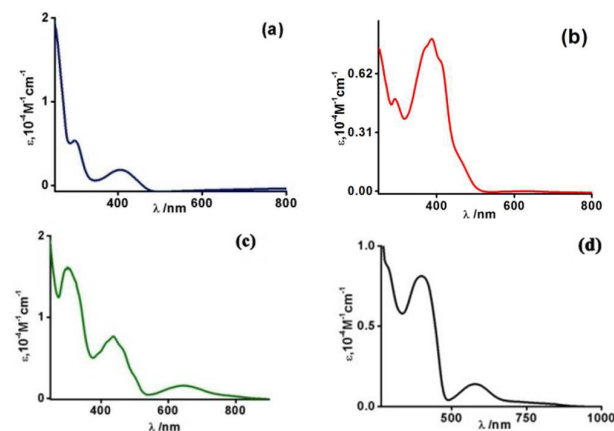


Fig. 9 UV-vis spectra of (a) gmma , (b) **1**, (c) **2** and (d) $\mathbf{3}^+\text{Cl}^-$ in CH_2Cl_2 at 298 K.

exhibits bands at 406 and 296 nm that are assigned to $\pi_{\text{Ar-SMe}} \rightarrow \pi^*$ transition (Fig. 9(a)). In **1**, the similar transitions are observed at 414 and 386 nm (Fig. 9(b)). The calculated wave lengths (λ_{cal}) for these transitions of **1** are 415.5 and 383.4 nm. In addition, **1** absorbs at 468 nm and the corresponding λ_{cal} are 453.3 and 443.0 nm (Table S4) due to $p_{\text{Cl}} \rightarrow \pi^*$ transitions. **2** absorbs at 648, 501 and 466 nm (Fig. 9(d)). The corresponding λ_{cal} are 646.1 and 492.1 nm respectively due to $d_{\text{Ru}} \rightarrow \pi^*$ (MLCT type) and d_{Ru} to mixed- $d_{\text{Ru}}-\pi^*$ charge transfer (MMLCT) transitions. The UV-vis absorption spectra of $\mathbf{3}^+$ ion as shown in Fig. 9(e) is similar to that of **2**. In addition to an absorption maximum at 578 nm, $\mathbf{3}^+$ ion exhibits a NIR absorption band at 744 nm. The λ_{cal} due to the $d_{\text{Ru}} \rightarrow \pi^*$ transitions are 754.2 and 547.7 nm.

The UV-vis/NIR absorption spectra of $\mathbf{1}^-$, $\mathbf{2}^-$, $\mathbf{2}^+$ and **3** were recorded in CH_2Cl_2 by spectroelectrochemical measurements at 298 K and the spectral data are summarized in Table 3. The conversions occur via several isosbestic points. The absorption spectra of the $\mathbf{1} \rightarrow \mathbf{1}^-$ and $\mathbf{3}^+ \rightarrow \mathbf{3}$ conversions are shown in Fig. 10, other are illustrated in Fig. S9. One of the important features of the spectra of the reduced species is the decrease of the absorbance at the λ_{max} corresponding to the neutral analogues. It is due to the partial occupancy of the π^* orbitals in $\mathbf{1}^-$, $\mathbf{2}^-$ and **3** and $d_{\text{M}} \rightarrow \pi^*$ transitions are perturbed.

Table 3 UV-vis absorption spectral data of gmma , **1**, **2**, $\mathbf{3}^+\text{Cl}^-$, $\mathbf{1}^-$, $\mathbf{2}^-$, $\mathbf{2}^+$ and **3** in CH_2Cl_2 at 298 K

Comp	$\lambda_{\text{max}}/\text{nm}$ (ϵ , $10^4 \text{ M}^{-1} \text{ cm}^{-1}$)
gmma	406 (0.19), 296 (0.55)
1	608 (0.002), 468 (0.14) ^{sh} , 414 (0.67), 386 (0.80), 369 (0.75)
2	648 (0.16), 501 (0.26) ^{sh} , 466 (0.61) ^{sh} , 437 (0.77), 302 (1.6)
$\mathbf{3}^+\text{Cl}^-$	744 (0.05), 646 (0.15), 468 (0.5) ^{sh} , 435 (0.76), 301 (1.6) ^{sh}
$\mathbf{1}^-$	468 (0.10), 411 (0.52), 391 (0.59), 290 (0.50), 267 (0.82)
$\mathbf{2}^-$	654 (0.04), 434 (0.08) ^{sh} , 287 (0.30) ^{sh}
$\mathbf{2}^+$	650 (0.12), 416 (0.26) ^{sh} , 289 (0.59)
3	730 (0.05) ^{sh} , 575 (0.12), 395 (0.41), 287 (1.04) ^{sh}

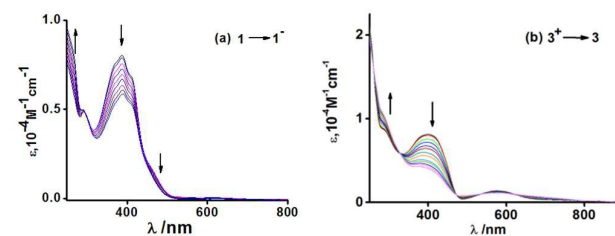


Fig. 10 Spectroelectrochemical measurements showing the change of electronic spectra during (a) $\mathbf{1} \rightarrow \mathbf{1}^-$ and (b) $\mathbf{3}^+ \rightarrow \mathbf{3}$ conversions in CH_2Cl_2 at 298 K.

Conclusion

In this article, the coordination chemistry of glyoxalbis(2-methylmercaptoanil) (gmma) which is a N_2S_2 donor α -diimine ligand, with nickel and ruthenium ions are disclosed. Nickel and ruthenium complexes of the types $\text{trans}[\text{Ni}^{\text{II}}(\text{gmma})\text{Cl}_2]$ (**1**), $\text{trans}[\text{Ru}^{\text{II}}(\text{gmma})\text{Cl}_2]$ (**2**) and $[\text{Ru}^{\text{II}}(\text{gmma})(\text{PPh}_3)\text{Cl}]^+\text{Cl}^-$ ($\mathbf{3}^+\text{Cl}^-$) are reported. The study authenticated that gmma is a redox non-innocent flexidentate ligand. **1** is a gmma complex of nickel(II), whereas $\mathbf{1}^-$ and $\mathbf{1}^{2-}$ ions are gmma^{+} and gmma^{2-} complexes of nickel(II). However both $\mathbf{1}^-$ and $\mathbf{1}^{2-}$ ions are not stable in solution and undergo a chemical change to a dinuclear species. In presence of PF_6^- ion, they afford a dinuclear square planer nickel(II) complex, $[(\mu\text{-NSNS-gmma})\text{Ni}_2\text{Cl}_3(\text{PF}_6)]$ ($\mathbf{4}^{\text{PF}_6}$) detected by ESI mass spectra, where $\mu\text{-NSNS-gmma}$ is a bis(methylthio-imine) donor bridging ligand.

With ruthenium the chemistry is different. The relatively longer C=N bonds of the diimine fragments propose a contribution of $[\text{Ru}^{\text{III}}(\text{gmma}^+)]$ state in **2** and $\mathbf{3}^+$ ion. $\mathbf{2}^-$ is a resonance hybrid of $\text{trans}[\text{Ru}^{\text{II}}(\text{gmma}^+)\text{Cl}_2]^-$ and $\text{trans}[\text{Ru}^{\text{III}}(\text{gmma}^{2-})\text{Cl}_2]^-$ states, while **3** is a resonance hybrid of $[\text{Ru}^{\text{II}}(\text{gmma}^+)(\text{PPh}_3)\text{Cl}]$ and $[\text{Ru}^{\text{III}}(\text{gmma}^{2-})(\text{PPh}_3)\text{Cl}]$ states. $\mathbf{2}^+$ is a neutral gmma complex of ruthenium(III). The study infers that the redox chemistry of gmma with harder nickel(II) ion is different from that of the softer ruthenium(II) ion. Thus, the redox and the structural chemistry of gmma with transition metal ion is a subject of investigation.

Acknowledgements

Financial support received from Department of Science and Technology (SR/S1/IC/0026/2012), Council of Scientific and Industrial Research (2699/12/EMR-II) and University Grants Commission (F. No. 43-214/2014(SR)) New Delhi, India is

ARTICLE

Journal Name

gratefully acknowledged. P.S. is thankful to CSIR, New Delhi, India, for fellowship (SRF) and D.S. gratefully acknowledged DST (SR/S1/IC/0026/2012) New Delhi, India, for fellowship. We sincerely acknowledge the support of Dr. Thomas Weyhermüller, Max-Planck-Institut für Chemische Energiekonversion, Germany to refine the X-ray structure of 3^+Cl^- .

References

- (a) L. Lecarme, L. Chiang, J. Moutet, N. Leconte, C. Philouze, O. Jarjayes, T. Storr and F. Thomas, *Dalton Trans.*, 2016, **45**, 16325-16334; (b) I. Pappas, S. Treacy and P. J. Chirik, *ACS Catal.*, 2016, **6**, 4105-4109; (c) O. R. Luca and R. H. Crabtree, *Chem. Soc. Rev.*, 2013, **42**, 1440-1459; (d) R. G. Hicks, *Nat. Chem.*, 2011, **3**, 189-191; (e) V. Lyaskovskyy and B. de Bruin, *ACS Catal.*, 2012, **2**, 270-279; (f) W. I. Dzik, J. I. van der Vlugt, J. N. H. Reek and B. de Bruin, *Angew. Chem. Int. Ed.*, 2011, **50**, 3356-3358; (g) P. J. Chirik and K. Wieghardt, *Science*, 2010, **327**, 794-795; (h) K. J. Blackmore, N. Lal, J. W. Ziller and A. F. Heyduk, *J. Am. Chem. Soc.*, 2008, **130**, 2728-2729; (i) W. Kaim, *Science*, 2005, **307**, 216-217.
- (a) F. Thomas, *Dalton Trans.*, 2016, **45**, 10866-10877; (b) D. L. J. Broere, R. Plessius and J. I. van der Vlugt, *Chem. Soc. Rev.*, 2015, **44**, 6886-6915.
- (a) C. W. Anderson, L. J. Rhinehart, G. A. Tennyson and K. B. Long, *J. Am. Chem. Soc.*, 2016, **138**, 774-777; (b) H. Mu, L. Pan, D. Song and Y. Li, *Chem. Rev.*, 2015, **115**, 12091-12137; (c) V. P. Ananikov, *ACS Catal.*, 2015, **5**, 1964-1971; (d) M. Brookhart, I. K. Goldberg and E. N. Gruhn, *ACS Catal.*, 2014, **4**, 1318-1319; (e) O. Daugulis, A. H. R. MacArthur, F. C. Rix and J. L. Templeto, *ACS Catal.*, 2012, **6**, 1518-1532; (f) S. K. Chatterjee, R. C. Maji, S. K. Barman, M. M. Olmstead and A. K. Patra, *Angew. Chem. Int. Ed.*, 2014, **53**, 10184-10189; (g) D. Meinhard, M. Wegner, G. Kipiani, A. Hearley, P. Reuter, S. Fischer, O. Marti and B. Rieger, *J. Am. Chem. Soc.*, 2007, **129**, 9182-9191; (h) B. L. Small, M. Brookhart and A. M. Bennett, *A. J. Am. Chem. Soc.*, 1998, **120**, 4049.
- (a) D. J. Blakemore, H. R. Crabtree and W. G. Brudvig, *Chem. Rev.*, 2015, **115**, 12974-13005; (b) D. M. Karkas, O. Verho, V. E. Johnston and B. Akermark, *Chem. Rev.*, 2014, **114**, 11863-12001; (c) L. Duan, F. Bozoglian, S. Mandal, B. Stewart, T. Privalov, A. Llobet and L. Sun, *Nat. Chem.*, 2012, **4**, 418-423; (d) P. Chaudhuri, M. Hess, T. Weyhermüller and K. Wieghardt, *Angew. Chem.*, 1999, **38**, 1095; (e) P. Chaudhuri, M. Hess, J. Müller, K. Hildenbrand, E. Bill, T. Weyhermüller and K. Wieghardt, *J. Am. Chem. Soc.*, 1999, **121**, 9599-9610.
- (a) W. W. Kramer, L. A. Cameron, R. A. Zarkesh, J. W. Ziller and A. F. Heyduk, *Inorg. Chem.*, 2014, **53**, 8825; (b) Q. Dong, J. -H. Su, S. Gong, Q. -S. Li, Y. Zhao, B. Wu and X. -J. Yang, *Organometallics*, 2013, **32**, 2866; (c) J. Gao, S. Li, Y. Zhao, B. Wu and X. -J. Yang, *Organometallics*, 2012, **31**, 2978; (d) A. Kochem, G. Gellon, O. Jarjayes, C. Philouze, A. du M. d'Hardemare, M. van Gastel and F. Thomas, *Dalton Trans.*, 2015, **44**, 12743-12756; (e) D. W. Shaffer, S. A. Ryken, R. A. Zarkesh and A. F. Heyduk, *Inorg. Chem.*, 2011, **50**, 13; (f) J. Gao, Y. Liu, Y. Zhao, X. -J. Yang and Y. Sui, *Organometallics*, 2011, **30**, 6071; (g) I. L. Fedushkin, O. V. Maslova, M. Hummert and H. Schumann, *Inorg. Chem.*, 2010, **49**, 2901; (h) I. L. Fedushkin, O. V. Eremenko, A. A. Skatova, A. V. Piskunov, G. K. Fukin, S. Y. Ketkov, E. Irran, and H. Schumann, *Organometallics*, 2009, **28**, 3863; (i) C. C. Lu, S. D. George, T. Weyhermüller, E. Bill, E. Bothe, K. Wieghardt, *Angew. Chem. Int. Ed.*, 2008, **74**, 6384-6387; (j) M. M. Khusniyarov, T. Weyhermüller, E. Bill and K. Wieghardt, *J. Am. Chem. Soc.*, 2009, **131**, 1208 and relevant references therein; (k) C. C. Lu, E. Bill, T. Weyhermüller, E. Bothe and K. Wieghardt, *J. Am. Chem. Soc.*, 2008, **130**, 3181-3197; (l) Y. Liu, P. Yang, J. Yu, X. -J. Yang, J. D. Zhang, Z. Chen, H. F. Schaefer and B. Wu, *Organometallics*, 2008, **27**, 5830; (m) H. Schumann, M. Hummert, A. N. Lukoyanov and I. L. Fedushkin, *Organometallics*, 2005, **24**, 3891; (n) R. J. Baker, R. D. Farley, C. Jones, M. Kloth and D. M. Murphy, *Chem. Commun.*, **2002**, 1196-1197; (o) K. Yang, R. J. Lachicotte and R. Eisenberg, *Organometallics*, 1998, **17**, 5102; (p) E. Rijnberg, B. Richter, K. -H. Thiele, J. Boersma, N. Veldman, A. L. Spek and G. van Koten, *Inorg. Chem.*, 1998, **37**, 56; (q) S. Greulich, A. F. Stange, H. Stoll, J. Fiedler, S. Zálíš and W. Kaim, *Inorg. Chem.*, 1996, **35**, 3998; (r) E. Rijnberg, J. Boersma, J. T. B. H. Jastrzebski, M. T. Lakin, A. L. Spektb and G. van Koten, *J. Chem. Soc., Chem. Commun.*, 1995, 1839; (s) M. G. Gardiner, G. R. Hanson, M. J. Henderson, F. C. Lee and C. L. Raston, *Inorg. Chem.*, 1994, **33**, 2456; (t) F. G. N. Cloke, C. I. Dalby, P. J. Daff and J. C. Green, *J. Chem. Soc. Dalton Trans.*, 1991, 181; (u) F. G. N. Cloke, C. I. Dalby, M. J. Henderson, P. B. Hitchcock, C. H. L. Kennard, R. N. Lamb and C. L. Raston, *J. Chem. Soc. Chem. Commun.*, 1990, 1394 and references therein; (v) W. Kaim, S. Ernst and V. Kasack, *J. Am. Chem. Soc.*, 1990, **112**, 173; (w) F. G. N. Cloke, G. R. Hanson, M. J. Henderson, P. B. Hitchcock, C. H. L. Kennard and C. L. Raston, *J. Chem. Soc., Chem. Commun.*, 1989, 1002; (x) J. Keijsper, G. van Koten, K. Vrleze, M. Zoutberg and C. H. Stam, *Organometallics*, 1985, **4**, 1306; (y) C. Creutz, *Comments Inorg. Chem.*, 1982, **1**, 293; (z) A. L. Balch and R. H. Holm, *J. Am. Chem. Soc.*, 1966, **88**, 5201.
- (a) S. K. Chatterjee, S. Roy, S. K. Barman, R. C. Maji, M. M. Olmstead and A. K. Patra, *Inorg. Chem.*, 2012, **51**, 7625-7635; (b) M. Ghosh, S. Sproules, T. Weyhermüller and K. Wieghardt, *Inorg. Chem.*, 2008, **47**, 5963; (c) N. Muresan, C. C. Lu, M. Ghosh, J. C. Peters, M. Abe, L. M. Henling, T. Weyhermüller, E. Bill and K. Wieghardt, *Inorg. Chem.*, 2008, **47**, 4579; (d) C. C. Lu, E. Bill, T. Weyhermüller, E. Bothe and K. Wieghardt, *Inorg. Chem.*, 2007, **46**, 7880; (e) N. Muresan, T. Weyhermüller and K. Wieghardt, *Dalton Trans.*, 2007, 4390.
- (a) D. Sellmann, S. Emig, F. W. Heinemann and F. Knoch, *Angew. Chem.*, 1997, **36**, 1201; (b) D. Sellmann, S. Emig and F. W. Heinemann, *Angew. Chem.*, 1997, **36**, 1734; (c) D. Sellmann, O. Kappler, F. Knoch and M. Z. Moll, *Naturforsch., B, Chem. Sci.*, 1987, **42b**, 1291; (d) Z. Dori, R. Eisenberg, E. I. Stiefel and H. B. Gray, *J. Am. Chem. Soc.*, 1970, **92**, 1506-1511.
- P. Ghosh, E. Bill, T. Weyhermüller, F. Neese and K. Wieghardt, *J. Am. Chem. Soc.*, 2003, **125**, 1293.
- (a) K. Takao, S. Tsushima, T. Ogura, T. Tsubomura and Y. Ikeda, *Inorg. Chem.*, 2014, **53**, 5772; (b) V. A. Piskunov, O. Y. Trofimova, K. G. Fukin, S. Y. Ketkov, I. V. Smolyaninov and V. K. Cherkasova, *Dalton Trans.*, 2012, **41**, 10970; (c) A. Saha Roy, M. Muresan, H. M. Tuononen, S. P. Rath and P. Ghosh, *Dalton Trans.*, 2008, 3438; (d) S. Kar, B. Sarkar, S. Ghumaan, M. Leboschka, J. Fiedler, W. Kaim and G. K. Lahiri, *Dalton Trans.*, 2007, 1934; (e) S. Kar, B. Sarkar, S. Ghumaan, D. Roy, F. A. Urbanos, J. Fiedler, R. B. Sunoj, R. J. Aparicio, W. Kaim and G. K. Lahiri, *Inorg. Chem.*, 2005, **44**, 8715; (f) E. Bayer and E. Breitmaier, *Chem. Ber.*, 1968, **101**, 1579.
- S. Chatterjee, S. Mandal, S. Samanta and S. Goswami, *Dalton Trans.*, 2012, **41**, 7057-7066.
- P. S. Hallman, T. A. Stephenson and G. Wilkinson, *Inorg. Synth.*, 1970, **12**, 237.
- (a) G. M. Sheldrick, *XS. Version 2013/1*, Georg-August-Universität Göttingen, Göttingen, Germany, 2013; (b) G. M. Sheldrick, *Acta crystallographica. Section A, Foundations and advances*, 2015, **71**, 3-8; (c) G. M. Sheldrick, *Acta*

- Crystallographica Section C Structural Chemistry*, 2015, **71**, 3-8.
- 13 M. J. Frisch, G. W. Trucks, H. B. Schlegel, G. E. Scuseria, M. A. Robb, J. R. Cheeseman Jr., J. A. Montgomery, T. Vreven, K. N. Kudin, J. C. Burant, J. M. Millam, S. S. Iyengar, J. Tomasi, V. Barone, B. Mennucci, M. Cossi, G. Scalmani, N. Rega, G. A. Petersson, H. Nakatsuji, M. Hada, M. Ehara, K. Toyota, R. Fukuda, J. Hasegawa, M. Ishida, T. Nakajima, Y. Honda, O. Kitao, H. Nakai, M. Klene, X. Li, J. E. Knox, H. P. Hratchian, J. B. Cross, V. Bakken, C. Adamo, J. Jaramillo, R. Gomperts, R. E. Stratmann, O. Yazyev, J. A. Austin, R. Cammi, C. Pomelli, J. W. Ochterski, P. Y. Ayala, K. Morokuma, G. A. Voth, P. Salvador, J. J. Dannenberg, V. G. Zakrzewski, S. Dapprich, A. D. Daniels, M. C. Strain, O. Farkas, D. K. Malick, A. D. Rabuck, K. Raghavachari, J. B. Foresman, J. V. Ortiz, Q. Cui, A. G. Baboul, S. Clifford, J. Cioslowski, B. B. Stefanov, G. Liu, A. Liashenko, P. Piskorz, I. Komaromi, R. L. Martin, D. J. Fox, T. Keith, M. A. Al-Laham, C. Y. Peng, A. Nanayakkara, M. Challacombe, P. M. W. Gill, B. Johnson, W. Chen, M. W. Wong, C. Gonzalez and J. A. Pople, *GAUSSIAN 03 (Revision E.01)*, Gaussian, Inc., Wallingford, CT, 2004.
 - 14 (a) D. R. Salahub and M. C. Zerner, *The Challenge of d and f Electrons*, *ACS Symposium Series 394*, American Chemical Society, Washington, DC, 1989; (b) R. G. Parr and W. Yang, *Density Functional Theory of Atoms and Molecules*, Oxford University Press, Oxford, UK, 1989; (c) W. Kohn and L. J. Sham, *Phys. Rev.*, 1965, **140**, A1133–A1138; (d) P. Hohenberg and W. Kohn, *Phys. Rev.*, 1964, **136**, B864–B871.
 - 15 (a) R. E. Stratmann, G. E. Scuseria and M. Frisch, *J. Chem. Phys.*, 1998, **109**, 8218–8224; (b) M. E. Casida, C. Jamoroski, K. C. Casida and D. R. Salahub, *J. Chem. Phys.*, 1998, **108**, 4439–4449; (c) R. Bauernschmitt, M. Haser, O. Treutler and R. Ahlrichs, *Chem. Phys. Lett.*, 1996, **256**, 454–464.
 - 16 (a) A. D. Becke, *J. Chem. Phys.*, 1993, **98**, 5648–5652; (b) B. Miehlich, A. Savin, H. Stoll and H. Preuss, *Chem. Phys. Lett.*, 1989, **157**, 200–205; (c) C. Lee, W. Yang and R. G. Parr, *Phys. Rev. B: Condens. Matter*, 1988, **37**, 785–789.
 - 17 P. J. Pulay, *Comput. Chem.*, 1982, **3**, 556.
 - 18 H. B. Schlegel, J. J. McDouall, in *Computational Advances in Organic Chemistry*, ed. C. Ogretir, I. G. Csizmadia, Kluwer Academic, The Netherlands, 1991, pp. 167–185.
 - 19 P. J. Hay and W. R. Wadt, *J. Chem. Phys.*, 1985, **82**, 270–283.
 - 20 W. R. Wadt and P. J. Hay, *J. Chem. Phys.*, 1985, **82**, 284–298.
 - 21 P. J. Hay and W. R. Wadt, *J. Chem. Phys.*, 1985, **82**, 299–310.
 - 22 (a) V. A. Rassolov, M. A. Ratner, J. A. Pople, P. C. Redfern and L. A. Curtiss, *J. Comput. Chem.*, 2001, **22**, 976–984; (b) P. C. Hariharan, J. A. Pople, *Mol. Phys.*, 1974, **27**, 209–214; (c) P. C. Hariharan and J. A. Pople, *Theor. Chim. Acta.*, 1973, **28**, 213–222; (d) W. J. Hehre, R. Ditchfield and J. A. Pople, *J. Chem. Phys.*, 1972, **56**, 2257–2261.
 - 23 (a) V. A. Rassolov, J. A. Pople, M. Ratner and T. L. Windus, *J. Chem. Phys.*, 1998, **109**, 1223; (b) M. M. Francl, W. J. Pietro, W. J. Hehre, J. S. Binkley, D. J. DeFrees, J. A. Pople and M. S. Gordon, *J. Chem. Phys.*, 1982, **77**, 3654–3665; (c) P. C. Hariharan and J. A. Pople, *Theoret. Chimica Acta.*, 1973, **28**, 213.
 - 24 N. M. O'Boyle, A. L. Tenderholt and K. M. Langner, *J. Comp. Chem.*, 2008, **29**, 839.
 - 25 (a) M. Cossi, N. Rega, G. Scalmani and V. Barone, *J. Comput. Chem.*, 2003, **24**, 669; (b) V. Barone and M. Cossi, *J. Phys. Chem. A*, 1998, **102**, 1995.
 - 26 (a) S. C. Patra, T. Weyhermüller and P. Ghosh, *Inorg. Chem.*, 2014, **53**, 2427; (b) S. C. Patra, A. Saha Roy, V. Manivannan, T. Weyhermüller and P. Ghosh, *Dalton Trans.*, 2014, **43**, 13731; (c) S. C. Patra, M. K. Biswas, A. N. Maity and P. Ghosh, *Inorg. Chem.*, 2011, **50**, 1331.
 - 27 A. Saha Roy, H. M. Tuononen, S. P. Rath and P. Ghosh, *Inorg. Chem.*, 2007, **46**, 5942.
 - 28 J. Krzystek, A. Ozarowski and J. Telser, *Coord. Chem. Rev.*, 2006, **250**, 2308–2324.
 - 29 G. Skara, M. Gimferrer, F. De Proft, P. Salvador and B. Pinter, *Inorg. Chem.*, 2016, **55**, 2185–2199.
 - 30 M. K. Biswas, S. C. Patra, A. N. Maity, S. C. Ke, T. Weyhermüller and P. Ghosh, *Dalton Trans.*, 2013, **42**, 6538.
 - 31 (a) A. Takaoka, M. E. Moret and J. C. Peters, *J. Am. Chem. Soc.*, 2012, **134**, 6695; (b) A. Takaoka, C. H. Laura, L. C. H. Gerber and J. C. Peters, *Angew. Chem.*, 2010, **122**, 4182 and relevant references therein.

Glyoxalbis(2-methylmercaptoanil) complexes of nickel and ruthenium: radical versus non-radical states

Pinaki Saha, Debasish Samanta and Prasanta Ghosh*

Graphical abstract

The molecular and electronic structures of nickel(II) and ruthenium(II) complexes of glyoxalbis(2-methylmercaptoanil) and their reduced and oxidized analogues are reported.

